Distributed Snow Process Modeling
An Image Processing Approach

R.E. DAVIS[1], J.C. MCKENZIE[1] AND R.E. JORDAN[1]

ABSTRACT

This paper reports on an approach to spatially distribute a snow process model by segmenting images of land cover, terrain and snow properties. A small 1.7-ha study area with an existing data base was selected for this preliminary evaluation. The methodology was carried out over a relatively flat valley bottom at Camp Grayling, Michigan. Meteorological measurements on two sides of the area showed only small differences, so uniform meteorological variables were assumed over the site. Initial snow cover conditions were reconstructed and distributed over the area using snow maps and sparse snow pit measurements. One-meter resolution terrain, soil, vegetation and snow type maps were individually processed into class maps. These layers were then combined to produce a segmented class map, where the attributes from the data layers were known for each class. A one-dimensional model of snow processes was run for each class; the results were then mapped back into images. Shallow snow conditions provided high sensitivity of ablation patterns to meteorological conditions over a 72-hour period. Model performance was assessed by comparing predicted and observed ablation patterns. Error in total snow-covered area was less than 9 percent. However, the location errors were greater (predicted snow where no snow was observed and observed snow where no snow was predicted). Extensive error analysis was not justified because of the lack of multiple point measurements of snow properties.

Key words: Energy transfer, Image processing, Snow modeling, Spatial distribution

INTRODUCTION

This paper reports a method of spatially distributing a snow process model over an area with variable terrain and land cover. The terrain, land cover and snow data were handled as images, which were geo-registered at the same resolution. Development of model strategies that fully distribute the inputs and outputs of snow models has been motivated by the need to predict higher spatial detail and more process-level detail than possible by using partially distributed or lumped parameter models. Many recent research efforts have generated data sets suitable for development and tests of fully distributed snow models (Dozier 1992). One-dimensional models of the energy and mass transfer of snow cover have become quite sophisticated, incorporating most of the process-level detail required by some modeling applications (see reviews by Colbeck 1987, Morris 1991, Dozier 1992). Kirnbauer et al. (1994) review recent approaches and discuss the limitations to the use of distributed snow models for predicting snowmelt runoff.

Spatially distributing one-dimensional snow models is usually done by defining a discrete set of land cover elements, regular square grid cells or polygonal areas with similar attributes (e.g. Leavesley and Stannard 1990) then running a point model for each of these elements. Processes or properties that have characteristic length scales greater than the size of the units are represented explicitly, while those with scales less than the discretized units must be parameterized (Kirnbauer et al. 1994, Blöschl and Sivapalan 1995). Within a landscape or response unit, processes over and within the snow cover are assumed laterally uniform. However, the length scale over which homogeneity can be demonstrated in the field is usually significantly less than the scale of the response classes in distributed modeling framework. Two reasons for this are the constraints placed by computing time and, more importantly, the scale of the supporting data sets. Therefore some level of parameterization is associated with distributed modeling, whether that necessary for large regular grid cells or understanding the variance within and between response classes.

Distributed snow models have usually been tested against a single variable, snowmelt runoff, measured at a catchment outlet. No spatial information is represented and the snow melting signal has been convolved by

[1] U.S. Army Cold Regions Research and Engineering Laboratory (CRREL), 72 Lyme Road, Hanover, New Hampshire 03755-1290 USA

a routing or signal processing scheme. Such tests represent a test of a basin water budget (initial snow water equivalent versus basin outflow), not a test of the model's ability to accurately mimic the distributed processes. Site-scale measurements have rarely been used for validation because of the prohibitive cost in acquiring sufficient quantities of measurements for robust statistics.

Spatial snow modeling should be compared with spatial information (e.g. Blöschl et al. 1991, Blöschl and Kirnbauer 1992). Maps of snow cover extent, for example, provide appropriate measures for initializing and evaluating distributed snow models. As methods are developed to recover other snow properties, such as snow grain size or water equivalent, from remote sensing measurements, there will be improved opportunities to thoroughly test distributed snow models. Ultimately, data to drive distributed snow models will likely consist of a combination of point and spatial measurements. Site-scale measurements must be interpolated and/or extrapolated over the terrain data. Spatial measurements will most likely consist of data layers derived from remote sensing observations.

The field study represents a limited test. First, the area (1.7 ha) has a scale that would be an entire response unit in a basin-scale study. Second, the existing data set was rich in spatial data, but poor in vertical measurements of snow properties. There are three potential sources of error in distributed snow modeling: 1) description of the snow cover on the terrain where the model is solved; 2) estimation of the spatial fields of meteorological variables for input to the model; and 3) methods by which the snow processes are represented in the model. The focus of this paper is on how land cover information can be handled as images for the purpose of defining classes where a one-dimensional snow model can be run. Therefore we used an existing data set so that errors from (2) were small, if not insignificant. In addition, we assume that errors due to (3) were also small because of the one-dimensional snow model we used (Jordan 1991).

METHODS

Test location and period

Measurements were obtained from a field test facility at Camp Grayling, Michigan [44.7°N. lat., 85.6°W. long.]. We used co-registered terrain, vegetation, soil and surface water maps, which were available at 1-m resolution. Daily snow maps were also available at the same resolution.

Our investigation was centered on one of six areas where extensive measurement suites were deployed. The central part of the area had boundaries running northwest-southeast and northeast-southwest, in a diamond pattern roped off to prevent disturbance. A subimage of the raster DEM was cropped, which formed a square region around the undisturbed area with north-south and east-west boundaries and dimensions 134 × 134 m (Fig. 1). Lying on a valley floor with low slope, the land cover consisted of dry grasses and a few small

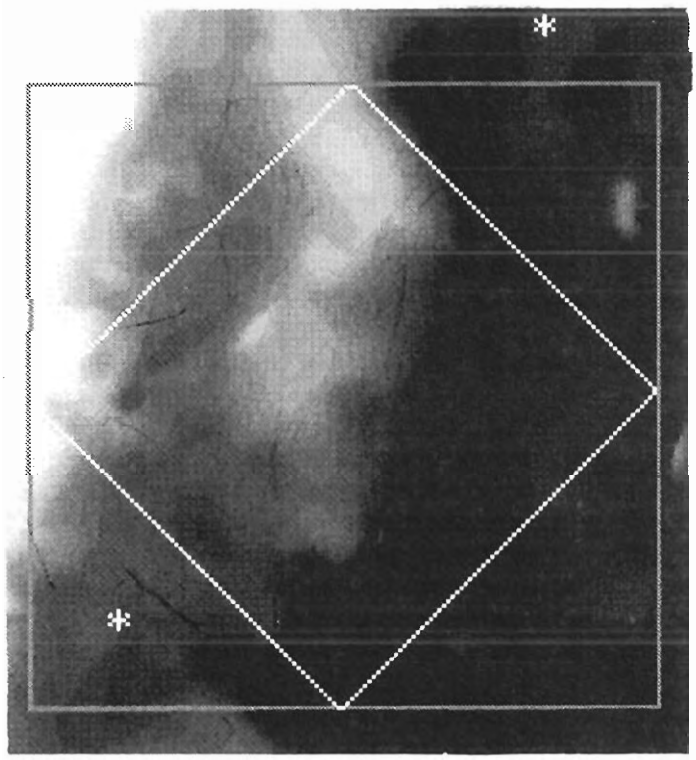

Figure 1. DEM of test area. Gray shades show relief of 6 m from white (upper left) to black (right). Actual elevation change is from 357 to 351 MSL. Asterisks show locations of meteorological stations. Gray square show test area; white diamond shows the undisturbed area. Scale: Diamond pattern is 100 × 100 m.

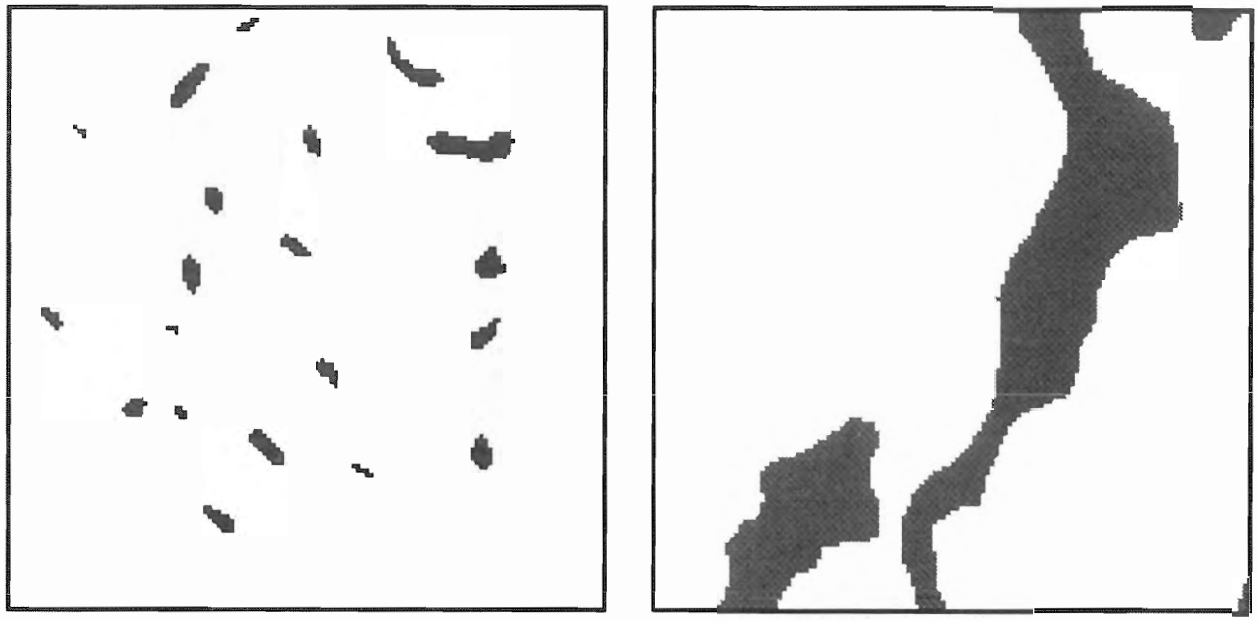

a. Grass (white) and trees (black). *b. Dry soil (white) and wet soil (dark gray).*

Figure 2. Vegetation and soil distributions on test area.

trees (black oak and pine) classified into two vegetation types (Fig. 2a). Two soil types were defined based on antecedent moisture content: nearly saturated and well drained, but at field capacity (Fig. 2b). Soil temperature profiles, measured by thermocouple arrays, also showed distinct differences between these two types. The wet soil type did not show as much change in the diurnal profile patterns as the dryer soil type.

A model test period of 72 hours was selected from an extensive data set, day of year (DY) 78–80 (March 19–21). We sought to compare model predictions of ablation pattern with the measured snow coverage. For this period there were adequate snow property measurements to initialize the model, old discontinuous snow with a period of snowfall, and a large change in snow-covered area.

Meteorological measurements

These variables control the energy and mass exchange above the surface of the snow, and are used to calculate to components of the surface energy exchange (Table 1).

Table 1. Meteorological variables in data set.

Air temperature
Relative humidity
Wind speed
Incoming solar radiation
Reflected solar radiation
Downwelling thermal infrared radiation
Precipitation, solid and liquid

Incoming radiation is modified in the model to account for slope and aspect. Precipitation was classed as snow if the air temperature is less than 0°C and rain if warmer (Jordan 1991).

Measurements were made of these variables at one-minute intervals at two stations within several meters of the test area (Fig. 1). These were compared to assess meteorological differences across the test area. Air temperatures at screen height (2 m above the soil) varied less than 1°C, between the stations except early during a storm when the wind speeds exceeded 5 m s^{-1}. During this period the larger differences ($\approx$ 3°C) occurred during rapid changes, which may reflect lateral advection of cold air from one instrument station to the other. Variations in relative humidity at the one-minute time step across the area likewise showed small differences. Differences in the wind speed, treated as a scalar quantity, were more pronounced. But variation was less than 5 m s^{-1} with most of the notable changes occurring during times of higher wind speeds. There was no systematic difference, variations occurred from one minute to the next. Hourly wind runs were quite similar in total distance. Solar and thermal radiation also showed small variations over the test period between the two meteorological stations, except during a snowstorm, when snow covered some of the sensors. The incoming thermal radiation showed little variation across the test area for the duration of the test period. With these comparisons there was no basis for selecting the measurements from one station or the other for input to the model simulations. Measurements from

the station to the northeast of the area were selected arbitrarily (Fig. 1).

During much of the test period the ground was bare underneath one or more of the radiometers while snow was present over the test area. Therefore, rather than using the ratio of incoming to reflected solar radiation from the measurements as albedo, we mapped albedo across the test area with the snow model by incorporating an algorithm relating albedo to the snow grain size. The algorithm caused a linear decay in albedo as a function of the square root of the grain radius, similar to the technique described by Marshal and Warren (1987).

Snow profile data

Snow pit measurements were attempted on a daily basis when snow was present at the test facility. As previously mentioned, the boundaries of the area were roped off, so that snow within the area would remain undisturbed. The location for each potential snow pit was determined by selecting a random distance and perimeter side (Fig. 1). When snow was found at the location, measurements were made, which included snow depth, density, grain size and liquid water content. Variables were reported for each significant depth in the snowpack. These measurements can be summarized in Table 2.

Table 2. Summary of ground cover and snow pit observations during test period.

DY 76: No snow at random location.
DY 77: Location near center of large snow patch, 18 cm total depth, new snow about 10 cm thick with densities ranging from 100–120 kg m^{-3}; old snow about 8 cm thick with density average about 280 kg m^{-3}.
Day 78: Location in area covered by new snow over previously bare ground, 8.5 cm total depth; density average about 170 kg m^{-3}.
Day 79: Location in area covered by new, but aging, snow over previously bare ground; 3.5 cm total depth; density average about 260 kg m^{-3}.
Day 80: No snow at random location.

Snow cover patterns

Snow cover maps were manually prepared each day. The procedure involved traveling around the area to reference points, then sketching the snow/no-snow boundary onto the base map. The same boundaries were observed and corrected from different vantage points. Hand-drawn snow maps were then digitized each day with a large digitizing board, onto the base map at a resolution of 1 m. Figure 3 depicts the time sequence of the snow cover pattern. Day of year 76 (upper left, Fig. 3) had scattered old melting snow. New snow-covered the area (upper right) on days 77

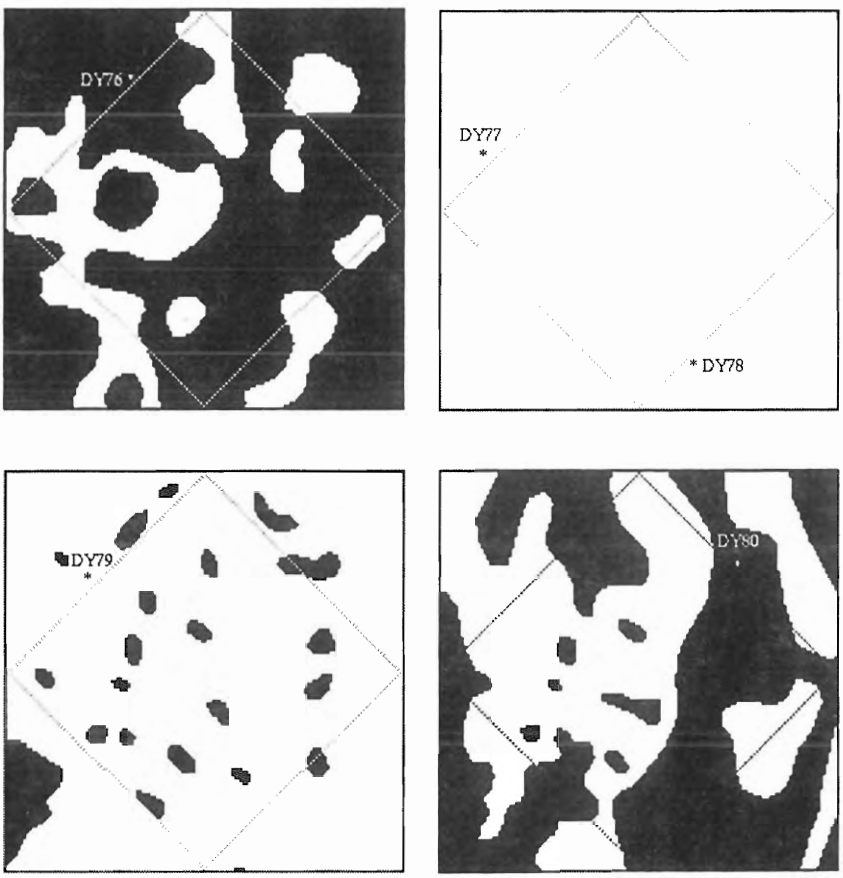

Figure 3. Observed snow-covered area. Five maps are represented along with locations of potential snow observations. Snow is white; bare ground is black.

Upper left–DY 76;
Upper right–DY 77 and DY 78;
Lower left–DY 79; and
Lower right–DY 80.

and 78. Snow began to melt out on DY 79 (lower left), and DY 80 was characterized by scattered melting snow (lower right).

Initial snow cover

To initialize the model run on DY 78, we constructed the image data set for the antecedent snow cover by using the snow map from DY 76 and the snow pit measurements of old snow properties from DY 77. Snow cover properties were treated as multiband images, where each band represented a specified height interval above the ground surface. The digital number (DN) in each pixel was scaled to the property of interest, such as density, so each image band represents a map of the property at the specified height interval. This means that we had an image stack for each property, density, grain size and so forth. Snow pit observations, density and grain size, from the old snow on DY 77 were binned into 2-cm increments. A maximum snow depth of the old snow was set to 10 cm, which was justified by anecdotal information from the field personnel. Applying this 5-layer profile to the snow map of DY 77 would have resulted in uniform snow properties everywhere. However, experience and information from the field area suggest that the snow depth increased from a minimum, at the edge of the snow cover, to the maximum depth in the central portion of the snow-covered areas. Therefore a tapering function of 2 cm m^{-2} was used to thicken the old snow from 2 cm, just inside the snow areas toward the maximum depth.

The incremental snow property images of the old snow from the basal layer upward show the erosion of the boundary pixels that resulted from the tapering process. Figure 4 shows the five images for density combined into one image representing a surface density map. Each gray level corresponds to the density of the top snow layer at that location. Older, denser layers (brighter gray levels) stick out at the edges from underneath deeper areas with new, lighter snow on top. The gray scales of the DN have been stretched to improve the appearance. Each gray level also corresponds to a 2-cm increment. Therefore, since five levels are shown, the maximum depth in the image is 10 cm. The patterns in this image (Fig. 4) were spatially identical to the grain size, temperature and snow class maps.

Meteorological measurements of precipitation were used to add snow to the antecedent cover. An initial density of 100 kg m^{-3} was used, so that the depth of water equivalent measured by the gage could be translated into snow depth. About 10 cm snow had accumulated by the morning of DY 78, which added 5 more images (at 2-cm height intervals) to the snow data set. The combination of methods to specify the initial snow cover resulted in six classes, identified by unique vertical profiles of properties. Figure 5 shows a conceptual side view. In this figure each layer is represented by a band in the image stack. The old snow, bounded by bold lines, is tapered, while the new snow forms uniform layers over the top.

Image data segmentation

The basis for distributing the model over the test area was a class map, or image, showing areas with unique combinations of the land cover features: classes of soil, vegetation, initial snow type, slope and aspect. Slope and aspect classes were arbitrarily specified to five and eight types respectively (Fig. 6). Each image in the combination was multiplied by a constant

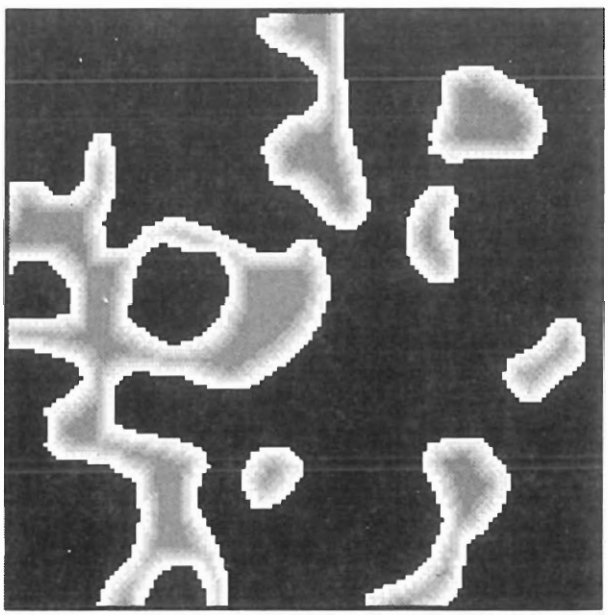

Figure 4. Combined image of snow cover layers on DY 76. Black represents no snow. Gray levels are scaled to density; lighter colors (higher DN) show higher densities. All snow in image is surface snow. Intervals of snow height farther up in the snow cover occupy less area. Therefore old, lower layers with higher densities (brighter) are seen extending out from the edges of the layers above.

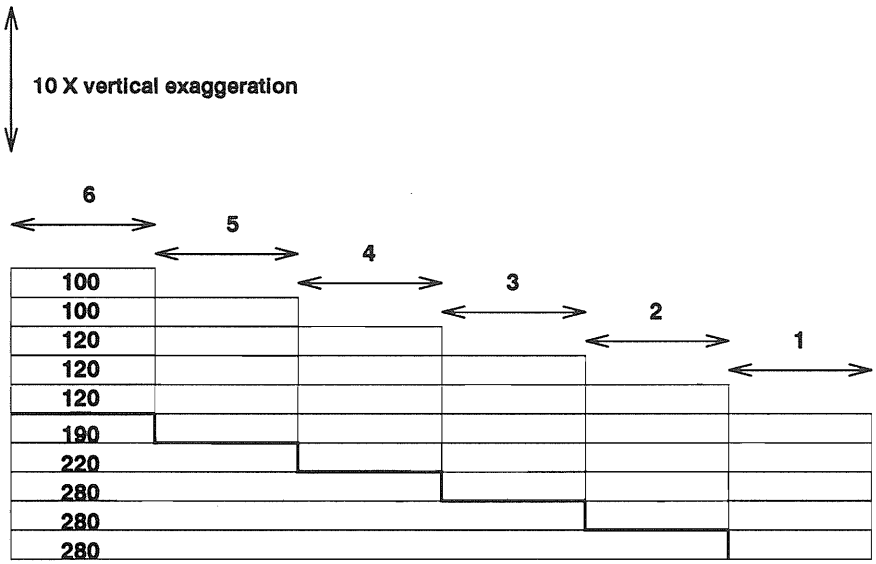

Figure 5. Conceptual side view of snow layer representation in imagery. Each layer is represented by a band in the imagery, where the extent of a height interval is stored as well as the property value (e.g., density, grain size, temperature, liquid water content).

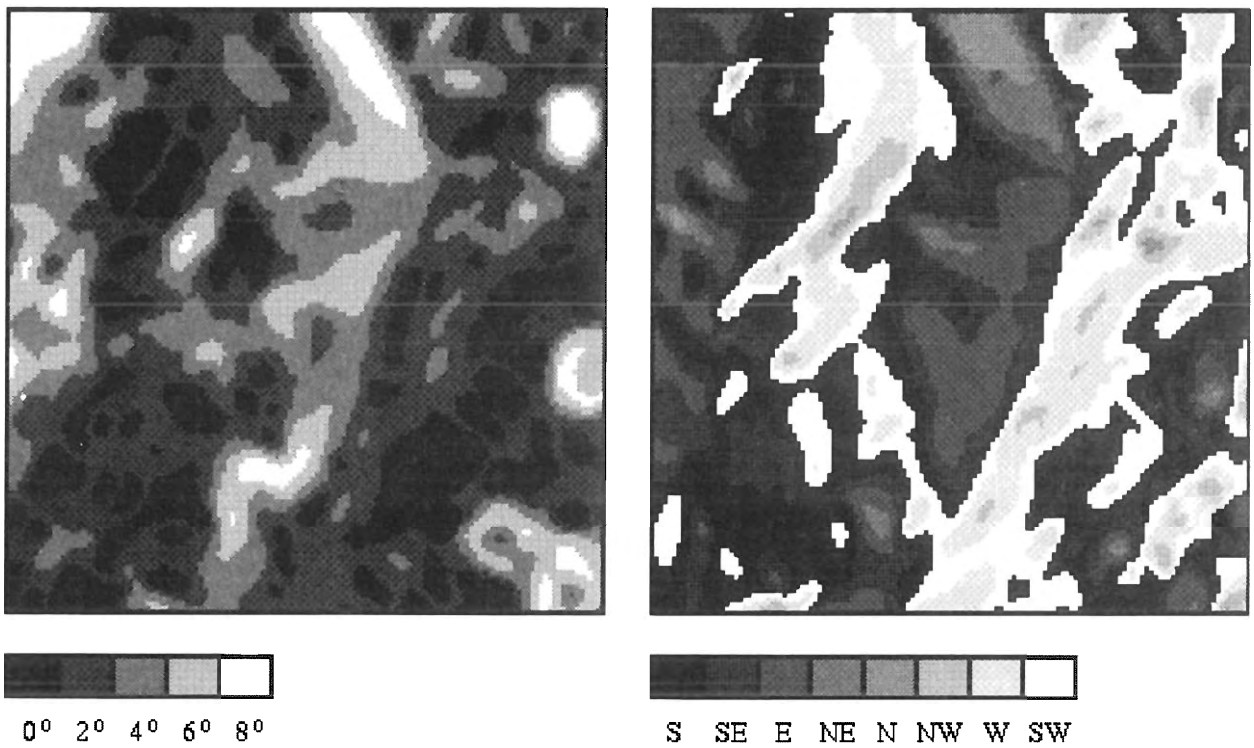

Figure 6. Slope and aspect classes. Slope (left) was generalized into five classes, each of which was centered on the angle shown (degrees). Aspect was generalized into eight directions (right).

so that the sums of the DN representing the classes resulted in unique numbers. An index table listing the total number of possible combinations of slope, aspect, soil, vegetation and snow was created from the image labels. This table had 960 potential combinations. Combinations that did not exist in the test area were identified from the class image by computing a histogram. Both the index table and the class images were then rescaled to eliminate nonexistent combinations and provide a continuous numbering scheme. This operation showed that only 351 classes were present. Most of the reduction came from the fact that the tree class on the vegetation image occupied little area, so not many of the possible combinations of snow and other land cover classes were associated. Inputs to the model were pointed to with the index table and runs were initialized and started. The model runs were sequentially numbered, so the results could be associated with the appropriate DN on the class image.

Point snow model

A one-dimensional mass and energy balance model, SNTHERM (Jordan 1991) was used to calculate the components of the surface energy exchange and the net energy budget, snow density, grain size, liquid water content and temperature in the snow layers. The model was initialized using measurements of the snow and soil physical properties. These included profiles of temperature, density and grain size, which were determined by observation. This model is comprehensive and can be used to simulate conditions found throughout the accumulation and ablation of a snowpack.

A one-dimensional numerical solution to the cross-coupled heat, water vapor and liquid water transport equations was realized by dividing the snow and soil layers into horizontal control volumes, each governed by the equations for heat and mass balance (Jordan 1991). The Crank-Nicolson method was used for discretizing the time domain and the spatial domain was discretized using a control-volume approach. Initial conditions were set by assigning properties to specific intervals of height relative to the ground surface for snow and intervals of depth for soil. The model predicts values of temperature, density, grain size and liquid water content for layers of varying thickness, depending on the processes of settlement, etc. During melting, for example, the top control volume decreased in thickness and was incorporated into the node underneath after losing thickness below a specified threshold. Similarly, a small threshold of depth was assigned to define the snow, no-snow condition in determining the final ablation of the last increment of snow.

MODEL RESULTS

Predictions of the distributed model run were compared with measurements at a point and over the test area. The predicted depth and vertical profiles of density and grain size were compared with a randomly located snow pit. The predicted snow cover ablation pattern was compared with the observed pattern on DY 80.

A single comparison of snow properties in vertical profile out of 17,956 1-m^2 pixels does not constitute a reasonable test. Nonetheless, we present the results since they offer our only comparison of model performance predicting properties at different height intervals for this test case. Snow pit observations on DY 79 were compared against the model predictions at the same location at the same time; the results are shown in Table 3.

Table 3. Comparison of observed and predicted snow properties.

	Depth	*Density*	*Grain radius*
Observed	3.5 cm	260 kg m^{-3}	1.0 mm
Predicted	2.5 cm	248 kg m^{-3}	0.7 mm

The location of the snow pit was an area that was bare ground before the storm on DY 77–78. After the storm, the model was initialized in that and other bare ground locations with 10 cm of new snow, with an average density of 112 kg m^{-3} and a grain size of 0.25 mm. The initial conditions were based on measurements from DY 77. The measurements of density and grain size were reported as averages for the layer. Snow depth were measured to the nearest 0.5 cm. The predicted snow depth was 1 cm less than the measured but the density and grain size were within the reported measurement error. This suggests that for this point at least the model ablated too much snow.

The observed and predicted snow cover patterns on DY 80 are shown in Figure 7. The total area of observed snow was 0.8981 ha (8981 pixels) and the total area of predicted snow was 0.9083 ha (9083 pixels). This represents a difference of less than 10 percent, with a total spatial error of 0.06 percent. Snow cover extent was observed to be much more spatially smooth and continuous (Fig. 7a) than the predicted results (Fig. 7b).

There are two kinds of locational error in this test: 1) predicted snow where no snow was observed and 2) observed snow where no snow was predicted. These errors, or residuals, are shown in Figure 8. The two kinds of error are roughly equally divided: the total area of error (1) was 0.3142 ha (17.5 percent of total area) and the total area of error (2) was 0.3244

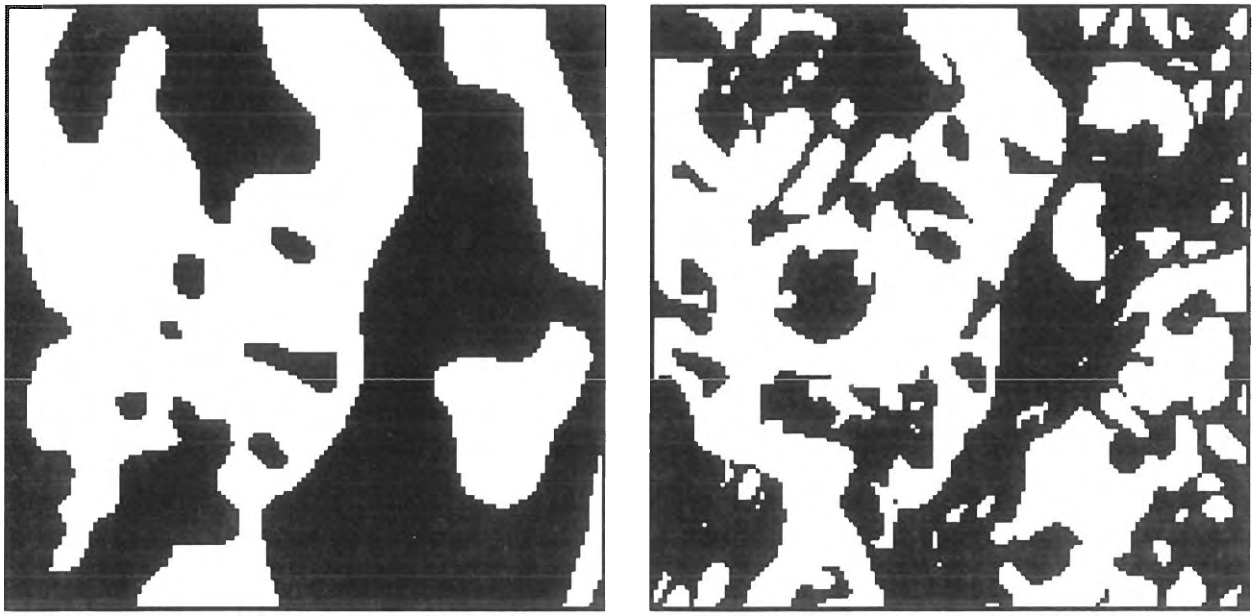

a. Manually drawn snow map from field observations. *b. Predicted snow extent.*

Figure 7. Observed and predicted snow cover patterns. Snow is white; bare ground is black.

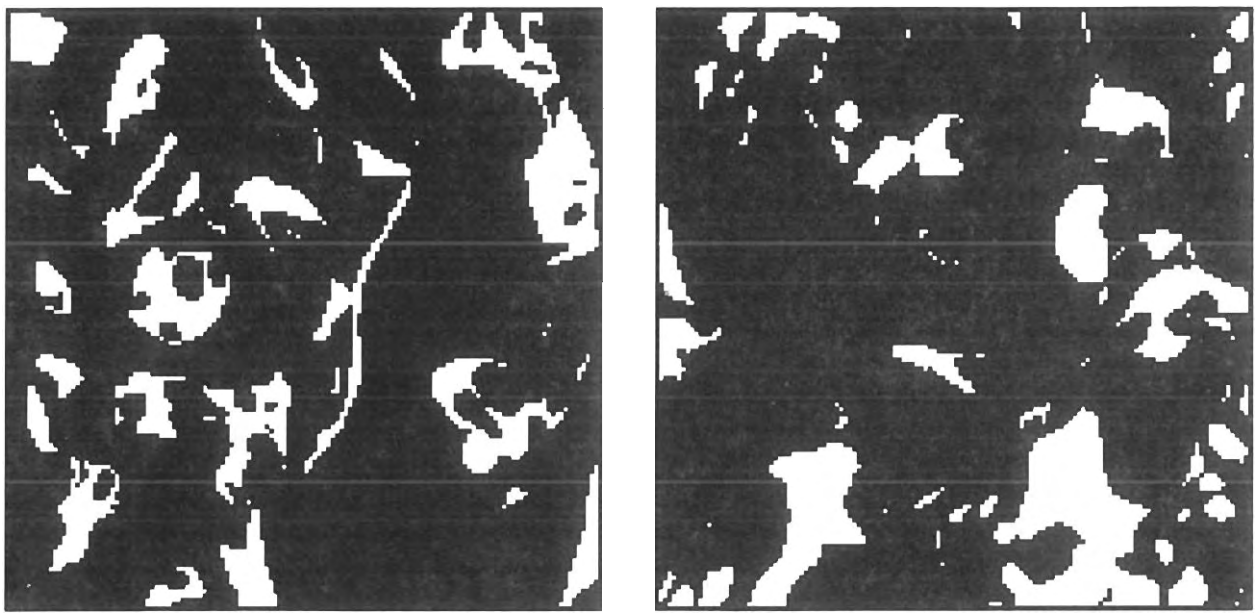

a. Areas of observed snow but no predicted snow. *b. Areas of predicted snow but no snow observed.*

Figure 8. Residuals of observed versus predicted snow cover comparison.

ha (18.1 percent of the total area). Thus the total locational error was 35.6 percent. The locational error was tabulated by class for each of the land cover classes, slope, aspect, soil, vegetation and snow. The error was proportional to the total area of each class. For example, the largest snow class was the area covered by new snow over bare ground. This class occupied 71 percent of the total area and accounted for 75 percent of the total locational error. Also in this class, the other residual error was almost evenly spread across slope and aspect classes. The errors for different types of class of these land cover attributes were about the same. The locational error was not random, but spatially correlated, as indicated by the sizes of the error areas. Further analysis was not warranted because of the lack of more point measurements of snow depth or properties.

DISCUSSION AND CONCLUSIONS

As previously described errors can arise from three main sources: 1) description of the snow cover on the terrain where the model is solved; 2) estimation of spatial fields of meteorological variables for input to the model; and 3) methods by which snow processes are represented. We sought to eliminate, or reduce to a low level, errors from sources (2) and (3) to focus on the representations of snow cover and land cover classes. The SNTHERM model is process-rich and has been tested and validated (cf. Jordan 1991, Clinton et al. 1995). We feel confident that variation in the surface energy exchange across the test area was uniform, except near the trees. Differences in snow accumulation around tree crowns due to canopy interception were not accounted for in the initial snow conditions. The effects of shadow of the trees were also not accounted for. Therefore most of the success, or error, in predicting the ablation patterns over the test area were probably due to the accuracy with which we specified the initial conditions. Better data for initializing and testing the model would have been a combination of many point measurements of depth-related properties and the maps of snow extent.

We used an existing data set from military research at CRREL, so we had no control on the experimental design. For preliminary tests with our focus we found no other data sets for which there were high resolution land cover maps and demonstratably uniform meteorological variables. We can now establish priorities for the types and amounts of experimental data that would be required for future experiments. The total number of classes run was 351, but the number of snow classes was 6. With many more point measurements, even of snow depth as a surrogate, the initial conditions of the snow cover could have been more detailed, possibly requiring fewer classes of the other land cover attributes. Daily snow maps were a critical element. Since spatial data offer more statistically robust tests, snow maps represent the minimum requirement for assessment. Locational errors can provide important clues to the sources of the error.

There are many methods by which data sets of land cover and snow properties can be aggregated into classes for point model runs. There are advantages and limitations to the method we described here. One advantage is that the class information for each data layer is explicitly controlled, provided that the information is scalar, such as slope, elevation and snow depth. Another advantage is that the upper limit on number of model runs is known at the start, although in our case this number dropped by almost two thirds. A major disadvantage is that the minimum and maximum areas of the classes that result when the data layers are combined are not known. This is troublesome if scaling tests are desired because size control of of solution classes then becomes site specific, requiring a trial and error process. Attractive alternatives to the methods we described include clustering, such as described recently by Harrington et al. (1995), hierarchical clustering, which allows region growing to specified tolerances (Woodcock and Harward 1992), and hybrid schemes involving both clustering and additive combinations. While the methods for arriving at a class map, or solution region image, may be changed, our image-based approach can still be used to handle input and output snow properties. Moreover, we explicitly represent the snow cover as three-dimensional, so if two- or three-dimensional snow models are desired, our data structure should be suitable.

ACKNOWLEDGMENTS

We wish to thank the helpful comments of Mary Albert, Susan Taylor, Walter Rosenthal and three anonymous reviewers. Steve Decato helped decipher the snow observations and provided invaluable anecdotal information about the site. This work was supported by U.S. Army Project 4A762784AT42.

REFERENCES

Blöschl, G., R. Kirnbauer and D. Gutnecht (1991) Distributed snowmelt simulations in an alpine catchment, 1. Model evaluation on the basis of snow cover patterns. *Water Resources Research*, **27**(12), 3171–3179.

Blöschl, G. and R. Kirnbauer (1992) An analysis of snow cover patterns in a small alpine catchment. *Hydrological Processes*, **6**: 99–109.

Blöschl, G. and M. Sivapalan (1995) Scale issues in hydrologic modeling. *Hydrological Processes*, **9**(3/4): 251–290.

Colbeck, S.C. (1987) History of snow cover research. *Journal of Glaciology*, Special Issue, p. 60–65.

Clinton, R.M., K.C. Kuivinen and R. Jordan (1995) Simulation of summer snowmelt on the Greenland ice sheet using a one-dimensional model. *Journal of Geophysical Research*, **100**(D8): 16,265–16,273.

Dozier, J. (1992) Opportunities to improve hydrologic data. *Reviews of Geophysics*, **30**(4): 315–331.

Frew, J.E. (1990) The image processing workbench. Ph.D. Thesis, Department of Geography, University of California, Santa Barbara.

Jordan, R. (1991) A one-dimensional temperature model for a snow cover, USA Cold Regions Research and Engineering Laboratory, Special Report, 91–16.

Kirnbauer, R., G. Blöschl and D. Gutknecht (1994)

Entering the era of distributed snow models. *Nordic Hydrology*, **25**: 1–24.

Harrington, R.F., K. Elder and R.C. Bales (1995) Distributed snowmelt modeling using a clustering algorithm,. In *Biogeochemistry of Seasonally Snow-Covered Catchments*. IAHS Publication 228, p. 167–174.

Leavesley, G. H. and L. G. Stannard (1990) Application of remotely sensed data in a distributed-parameter watershed model. In *Proceedings of Workshop on Applications of Remote Sensing Hydrology, Saskatoon, Saskachewan, Canada*. NHRI, p. 47–64.

Marshal, S.E. and S. G. Warren 1987, Parameterization of snow albedo for climate models. In *Large-Scale Effects of Seasonal Snow Cover*. IAHS Publication 166, 4p. 3–50.

Morris, E. M. (1991) Physics-based models of snow. In *Recent Advances in the Modelling of Hydrologic Systems*. Kluwer Academic Publishers, p. 85–112.

Woodcock, C. E. and V. J. Harward (1992) Nested-hierarchical scene models and image segmentation. *International Journal of Remote Sensing*, **13**(16): 3167–3187.